2024 IEEE 35th International Symposium on Personal, Indoor and Mobile Radio Communications (PIMRC) | 979-8-3503-6224-4/24/$31.00 ©2024 IEEE | DOI: 10.1109/PIMRC59610.2024.10817432

RIS phase optimization for Near-Field 5G Positioning: CRLB Minimization

Carla Macías
Department of Signal Theory and Communications
Universitat Politècnica de Catalunya
Barcelona, Spain
Email: carla.macias@upc.edu

Montse Nájar
Department of Signal Theory and Communications
Universitat Politècnica de Catalunya
Barcelona, Spain
Email: montse.najar@upc.edu

Pau Closas
Department of Electrical and Computer Engineering
Northeastern University
Boston, Massachusetts
Email: closas@ece.neu.edu

***Abstract*—This article addresses near-field localization using Reconfigurable Intelligent Surfaces (RIS) in 5G systems, where Line-of-Sight (LOS) between the base station and the user is obstructed. We propose a RIS phase optimization method based on the minimization of the Cramér-Rao Lower Bound (CRLB) for position estimation. The main contributions of the article are: (1) the derivation of the CRLB to optimize the RIS configuration; and (2) the application of the mentioned framework in near-field considering reflective RIS. The proposed method is validated with simulations, showing an accuracy improvement of RIS phase optimization with respect to the state-of-the-art methods.**

I. Introduction

The interaction between the digital and the physical world is becoming increasingly important in the context of telecommunications, as more and more devices are being developed to bridge the gap between these two domains. One of the key requirements for this interaction is high-definition situational awareness, which refers to the ability of a device to determine its own location in a given environment.

With 4G systems, a location accuracy of the order of 10 meters can be achieved [1]. However, with the use of 5G signals, a location accuracy of 1 meter can be achieved due to the use of larger bandwidths and higher carrier frequencies. Beyond 5G systems, the trend is to operate at much higher frequencies, benefit from large available bandwidths and, therefore, achieve an even higher localization accuracy. Nevertheless, transmissions at high carrier frequencies imply the appearance of obstructions due to objects blocking the Line-of-Sight (LoS) path between the transmitter and the receiver. [2] The blockage of the LoS and the issues associated with the Received Signal Strength (RSS) localization method [3] [4] constitute two key challenges for the localization accuracy improvement.

With these challenges in mind, the use of Reconfigurable Intelligent Surfaces (RIS) can effectively assist the base station (BS) with the user equipment's (UE) localization task, overcoming the first of the aforementioned issues [5] [6]. By introducing a RIS in our transmission framework, the path loss between the UE and the BS can be importantly reduced, as shown in Figure 1. In addition, the RIS can modify the impinging electromagnetic waves induced by the environment, avoiding them to interfere with the transmitted signal [7] [8].

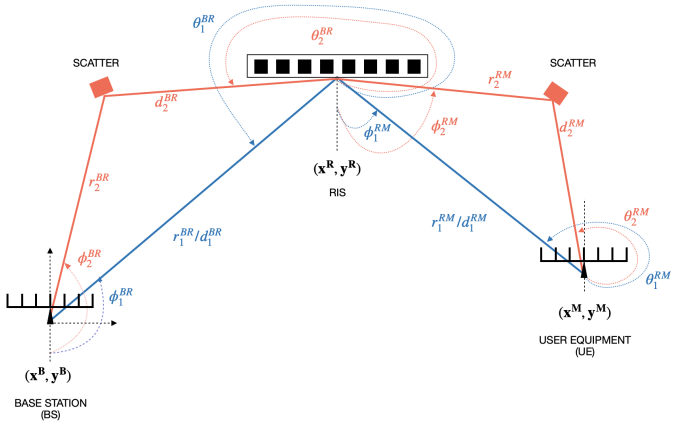

Fig. 1: Proposed architecture with the aid of a RIS where the LoS between the BS and UE is blocked. $\mathbf{p^B} = [x^B, y^B]$ and $\mathbf{p^R} = [x^R, y^R]$ are the known locations of the BS and RIS respectively, $\mathbf{p^M} = [x^M, y^M]$ is the unknown and to-be-estimated UE position. r^{BR} and r^{RM} are the distances between (the BS and the scatters) and (the RIS and the scatters) respectively and d^{BR} and d^{RM} are the distances between (the scatters and the RIS) and (the scatters and the UE) respectively. ϕ^q and θ^q are the angles of departure and angles of arrival of the different paths, being q the BR or RM path.

Therefore, RIS has become a promising technology, and it has been applied in various fields. For example, [9] proposes a RIS-aided hierarchical codebooks method for mmWave localization system. [10] proposed an architecture for joint communication and UE localization and orientation estimation in a RIS-assisted environment. [11] investigates the influence of different beamforming strategies for localization performance when RIS acting as Lens and proposes the corresponding maximum likelihood (ML) estimators.

Several contributions have been focusing on exploiting the problem of localizing user equipment (UE) using RIS. The authors in [12] studied the limits of mmWave MIMO positioning with the aid of a single RIS with a uniform linear array (ULA) for a two-dimensional positioning system. This work was extended to a three-dimensional scenario with a planar RIS in [13]. Furthermore, various articles studied different RIS phase design in order to improve the localization accuracy

979-8-3503-6224-4/24/$31.00 ©2024 IEEE

[14], [15].

This article develops on near-field localization using RIS, in 5G systems where LoS between the BS and the UE is obstructed. The main goal is to enhance the estimation of the UE position with respect to the BS, through the selection of convenient RIS phases. We propose a phase optimization method (for the computation of these RIS phases) based on the minimization of the Cramér-Rao Lower Bound (CRLB) of the UE positioning estimation.

The authors in [15] propose a framework to localize a UE in a near-field scenario, using a RIS system as well. However, their computation of the optimal RIS phases is based on the SNR maximization at the BS. This alternative method, which we will refer to as *Max. SNR method*, will work as our main baseline for performance comparison.

The main contributions of this article are: 1) The derivation of the CRLB to optimize the RIS configuration; 2) The application of the mentioned framework in near-field scenarios considering reflective RIS; and 3) a simulation-based experimental analysis showing that the proposed RIS phase optimization approach outperforms state-of-the-art solutions.

The remainder of the paper is organized as follows. Section II-A introduces the problem formulation, notation, and the employed localization algorithm. Section III presents the technical contribution of the article, deriving the CRLB of interest and comparing it to the alternative solution where the SNR is maximized. Section IV discusses the experiments that validate the proposed methodology and Section V conclude the paper with final remarks.

II. Background

This section provides a description of the system model and a formulation of the near-field 5G positioning problem. Additionally, a subsection describes the localization algorithm used in combination with the proposed RIS phase optimization method.

A. System Model

The architecture schema is presented in Figure 1. All components are equipped with multiple-input multiple-output (MIMO) uniform linear arrays (ULAs) with a number of elements N^B, N^R, N^M, for the BS, RIS and UE respectively. [16] The system model can be expressed as,

$$\mathbf{Y} = \mathbf{H}\mathbf{X} + \mathbf{Z} \tag{1}$$

where $\mathbf{Y} \in \mathbb{C}^{N^B \times M^0}$ is the received signal, $\mathbf{X} \in \mathbb{C}^{N^M \times M^0}$ is the Positioning Reference Signal (PRS) composed by orthogonal column pilots having M^0 sequences with power P, and $\mathbf{Z} \in \mathbb{C}^{N^B \times M^0}$ is an Additive White Gaussian Noise (AWGN) of zero mean and variance σ^2. The matrix $\mathbf{H} \in \mathbb{C}^{N^B \times N^M}$ is the channel matrix, which can be expressed as

$$\mathbf{H} = \mathbf{H}^{BR}\mathbf{\Omega}\mathbf{H}^{RM} \tag{2}$$

where $\mathbf{\Omega} \in \mathbb{C}^{N^R \times N^R}$ is a diagonal matrix with elements $\Theta = [\xi_1 e^{j\theta_1}, ..., \xi_{N_R} e^{j\theta_{N_R}}]$ with ξ_j and θ_j being the amplitudes and the RIS phases respectively (we will assume amplitudes $\xi_j = 1$), $\mathbf{H}^{BR} \in \mathbb{C}^{N^B \times N^R}$ is the channel between the BS and RIS and $\mathbf{H}^{RM} \in \mathbb{C}^{N^R \times N^M}$ is the channel between the RIS and UE. These channels are defined as follows:

$$\mathbf{H}^{BR} = \mathbf{A}(\phi^{BR}, r^{BR})\text{diag}(\rho^{BR})\mathbf{A}^H(\theta^{BR}, d^{BR}) \tag{3}$$

where $\mathbf{A}(\phi^{BR}, r^{BR}) \in \mathbb{C}^{N^B \times L^{BR}}$, $\text{diag}(\rho^{BR}) \in \mathbb{C}^{L^{BR} \times L^{BR}}$ and $\mathbf{A}(\theta^{BR}, d^{BR}) \in \mathbb{C}^{N^R \times L^{BR}}$ (with L^{BR} and L^{RM} being the number of paths between the BS and the RIS, and between the RIS and the UE respectively). The channel $\mathbf{H}^{RM}$ can be obtain analogously as.

$$\mathbf{H}^{RM} = \mathbf{A}(\phi^{RM}, r^{RM})\text{diag}(\rho^{RM})\mathbf{A}^H(\theta^{RM}, d^{RM}) \tag{4}$$

with similar matrix definitions.

Given that a near-field scenario is considered, the elements of the steering matrices $\mathbf{A}$ can be obtained using the Fresnel approximation of the spherical wavefront model [17] as follows,

$$a_{t,l}(\alpha_l^q, s_l^q) = e^{j(t\omega(\alpha_l^q) + t^2\gamma(\alpha_l^q, s_l^q))}$$
$$\text{with} \begin{cases} \omega(\alpha_l^q) = -\frac{2\pi\delta}{\lambda}\sin(\alpha_l^q) \\ \gamma(\alpha_l^q, s_l^q) = \frac{\pi\delta^2}{\lambda s_l^q}\cos^2(\alpha_l^q) \end{cases} \tag{5}$$

where λ is the wavelength, δ is the distance between two adjacent elements in the ULA. Notice that Equation 5 is a general expression that applies to each of the two channels. We expressed it in a compact form where superindex q can be either the BR or RM paths, $\alpha \in \{\phi, \theta\}$ and $s \in \{r, d\}$.

More specifically, the parameters defining the BR channel are such that $q = BR$, $t = b$ where $b \in \widetilde{B}$, $\widetilde{B} = [-B, .., B]$ and $B \doteq \frac{(N^B - 1)}{2}$. On the other hand, for the RM channel, the parameters are: $q = RM$ and $t = m$ where $m \in \widetilde{M}$, $\widetilde{M} = [-M, .., M]$ and $M \doteq \frac{(N^M - 1)}{2}$, with l denoting the corresponding path.

Finally, the propagation gain of each path ρ^q is represented as,

$$\rho^q = \left(\frac{c}{4\pi(r^q + d^q)f_c}\right)^{\mu/2} F \tag{6}$$

where c as the speed of light, f_c is the carrier frequency and F represents the fading coefficient [15].

B. Localization Algorithm

Building upon the signal model outlined in subsection II-A, this section introduces the algorithm to estimate the position of the UE. To do so, we first estimate the geometry-related parameters, including steering angles (ϕ_l^q and θ_l^q) and distances (r_l^q and r_l^q) derived from the received signal. This estimation process can be achieved, for instance, through Compressed Sensing (CS) [18] techniques.

Given the near-field nature of our scenario, applying CS directly over Equation 1 results in a high computational complexity problem, due to having to optimize over a grid of angles and distances.[1] For the sake of simplicity, [15] proposes

[1]Notice that, if far-field was considered instead, the gridding would only be performed over angles.

to exploit the spatial correlation in the channel matrix $\mathbf{H}$ to perform this gridding. To do so, matrix $\mathbf{V}$ is defined as a proper selection of elements from the covariance matrix of $\mathbf{H}$ [19]:

$$\begin{aligned} v_{b,m} &\doteq \mathbb{E}\left\{h_{b,m}{h_{p,n}}^*\right\} \\ \forall m \in \widetilde{M},\ b \in \widetilde{B},\ p = -b,\ n &= -m \end{aligned} \tag{7}$$

Multiple sparse estimation techniques can be used to estimate angles and distances. In this work, Orthogonal Matching Pursuit (OMP) has been considered as a recovery algorithm [20]. The remainder of the subsection details the four main steps required by the localization algorithm:

*1) **Estimation of** ϕ^{BR}:* $\mathbf{V}$ can be written as

$$\mathbf{V} = \mathbf{S}_1(\phi^{BR})\mathbf{C}_1 \tag{8}$$

where $\mathbf{V} \in \mathbb{C}^{B\times M}$, $\mathbf{S}_1 \in \mathbb{C}^{B\times N}$ and $\mathbf{C}_1 \in \mathbb{C}^{N\times M}$. $\mathbf{C}_1$ is an L^{BR}-sparse matrix[2].

The gridded matrix $\mathbf{S}_1 \in \mathbb{C}^{B\times N}$ is defined as $s_{b,n} = e^{2jb\omega(\phi_n^{BR})}$, which is basically a combination of N atoms each associated with an angle $\phi_n^{BR} = \frac{2\pi n - \pi(N+1)}{N-1}$ (where n is the grid counter and N is the grid size).

Applying the OMP recovery algorithm one can estimate $\hat{\phi}_{BR}$ [21] by finding the indices of the non-zero rows over $\mathbf{C_1}$ (recall it is L^{BR}-sparse).

*2) **Estimation of** $\theta^{\mathbf{RM}}$:* In this case, we consider

$$\mathbf{V}^H = \mathbf{S}_2(\theta^{RM})\mathbf{C}_2 \tag{9}$$

where $\mathbf{C}_2 \in \mathbb{C}^{N\times B}$ ($\mathbf{C}_2$ is L^{RM}-sparse as well). Analogously, $\hat{\theta}^{RM}$ can be estimated constructing the gridded measurement matrix $\mathbf{S}_2 \in \mathbb{C}^{M\times N}$ with elements $s_{m,n} = e^{-2jm\omega(\theta_n^{RM})}$ and selecting the indices of the non-zero rows from $\mathbf{C}_2$, as done in subsection II-B1.

*3) **Estimation of** r^{BR} **and** d^{RM}:* To estimate the distance $\hat{r}^{BR}$ the following relation is employed,

$$\mathbf{Y} = \mathbf{A}(\hat{\phi}^{BR}, \mathbf{r^{BR}})\mathbf{C}_3 \tag{10}$$

where $\mathbf{C}_3 \in \mathbb{C}^{N\times M}$ and $\mathbf{A}(\hat{\phi}^{BR}, \mathbf{r^{BR}})$ is the gridded matrix over the estimated angle $\hat{\phi}^{BR}$ and the distance vector $\mathbf{r^{BR}}$, which is upper bounded by the Fraunhofer distance $d_F = \frac{2D^2}{\lambda}$. [22] Analogously, $\hat{d}^{RM}$ can be obtained from

$$\mathbf{Y}^H = \mathbf{X}^H\mathbf{A}(\hat{\theta}^{RM}, \mathbf{d^{RM}})\mathbf{C}_4 \tag{11}$$

where $\mathbf{C}_4 \in \mathbb{C}^{N\times B}$.

*4) **Positioning**:* The position of the BS has been considered as the reference frame and, from the estimated parameters, it is possible to obtain the UE location as

$$\begin{aligned} \hat{x}^M &= x^R + \hat{r}_l^{RM}\sin(\hat{\phi}_l^{RM}) + \hat{d}_l^{RM}\sin(\hat{\theta}_l^{RM}) \\ \hat{y}^M &= y^R + \hat{r}_l^{RM}\cos(\hat{\phi}_l^{RM}) - \hat{d}_l^{RM}\cos(\hat{\theta}_l^{RM}) \end{aligned} \tag{12}$$

[2]An L-sparse matrix is such that it only contains L non-zero rows.

III. CRLB-BASED RIS PHASE OPTIMIZATION

The objective of this article is to improve the accuracy of the user's position estimation by minimizing its average distortion with Euclidean distance measure [10], that is to minimize the mean square error (MSE)

$$\mathrm{MSE}(\boldsymbol{\xi}, \hat{\boldsymbol{\xi}}) = \mathbb{E}\left[(x^M - \hat{x}^M)^2\right] + \mathbb{E}\left[(y^M - \hat{y}^M)^2\right] \tag{13}$$

where $\boldsymbol{\xi} = \left[x^M, y^M\right]^\top$ is the vector of the unknown parameters.

A. Maximization of the SNR

One way to optimize system performance is by maximizing the signal-to-noise ratio (SNR), which has a significant impact on minimizing the MSE. To do so, various methods can be used, one of which involves aligning the phases at the BS, as presented in [15]. As a result, a closed-form solution for the phases can be obtained as:

$$\begin{aligned} \theta_r^* = &\Big((2M+1)(2B+1)L^{BR}L^{RM}\Big)^{-1}\sum_{b,m}\Big[b\omega(\hat{\phi}^{BR}) \\ &+ b^2\gamma(\hat{\phi}^{BR}, \hat{r}^{BR}) + r\omega(\hat{\theta}^{BR}) + r^2\gamma(\hat{\theta}^{BR}, \hat{d}^{BR}) \\ &+ r\omega(\hat{\phi}^{RM}) + r^2\gamma(\hat{\phi}^{RM}, \hat{r}^{RM}) + m\omega(\hat{\theta}^{RM}) \\ &+ m^2\gamma(\hat{\theta}^{RM}, \hat{d}^{RM})\Big], \quad \forall r \in (1, \ldots, N^R) \end{aligned} \tag{14}$$

B. Minimization of the CRLB

In this work we propose an alternative phase optimization method based on the minimization of the positioning CRLB in a near-field scenario that takes into account the presence of a RIS channel. In comparison to the aforementioned SNR method, this approach offers a tighter connection to the problem of minimizing the MSE [10]. In our case, the objective is to find the RIS phases that provide the minimum theoretically attainable value for the standard deviation of the positioning estimation (for unbiased estimators), i.e.

$$\mathrm{MSE}(\boldsymbol{\xi}, \hat{\boldsymbol{\xi}}) \geq \mathrm{tr}(\mathbf{J}_\xi^{-1}) \tag{15}$$

where $\mathbf{J}_\xi$ denotes their Fisher Information Matrix (FIM).

We first compute the FIM of the parameters $\boldsymbol{\eta} = [d^{RM}, r^{RM}, \phi^{RM}, \theta^{RM}]^\top$, denoted as $\mathbf{J}_\eta$, where the estimation of $\boldsymbol{\eta}$ can be interpreted as $\hat{\boldsymbol{\eta}} = \boldsymbol{\eta} + \mathbf{w}$, with $\mathbf{w} \sim \mathcal{N}(\mathbf{0}, \boldsymbol{\Sigma})$ as a complex normal estimation error of zero mean and variance $\boldsymbol{\Sigma}$. In this work $\hat{\boldsymbol{\eta}}$ has been obtained using CS techniques, e.g. orthogonal matching pursuit as discussed in subsection II-B.

For the sake of simplicity, from this point on we will not be considering scatters, and our framework will only take into account the direct path from the BS to the RIS and from the RIS to the UE. Hence, $r_1^{RM} = d_1^{RM}$, $\theta_1^{RM} = \pi + \phi_1^{RM}$ and our estimated position becomes,

$$\begin{aligned} \hat{x}^M &= x^R + \hat{r}^{RM}\sin(\hat{\phi}^{RM}) \\ \hat{y}^M &= y^R - \hat{r}^{RM}\cos(\hat{\phi}^{RM}) \end{aligned} \tag{16}$$

We aim to calculate the CRLB for the vector $\boldsymbol{\xi}$. Therefore, we first calculate the FIM of $\boldsymbol{\eta}$ and then perform a transformation for $\boldsymbol{\xi}$:

$$[\mathbf{J}_\eta]_{i,j} = \Psi(\eta_i, \eta_j) = \frac{P}{\sigma^2}\mathbb{R}\left\{\text{tr}\Big(\frac{\partial \mathbf{\Pi}^H}{\partial \eta_i}\frac{\partial \mathbf{\Pi}}{\partial \eta_j}\Big)\right\} \tag{17}$$

where, SNR $= \frac{P}{\sigma^2}$ and

$$\mathbf{\Pi} = \mathbf{H}^{BR}\mathbf{\Omega}\mathbf{H}^{RM}\mathbf{X} \tag{18}$$

The detailed derivatives of $\mathbf{\Pi}$ with respect to the four elements in $\boldsymbol{\eta}$:

$$\frac{\partial \mathbf{\Pi}}{\partial d^{RM}} = \mathbf{H^{BR}\Omega A}(\phi^{RM}, r^{RM})\Big[\frac{\partial \rho^{RM}}{\partial d^{RM}}\mathbf{A}^H(\theta^{RM}, d^{RM}) + \rho^{RM}\frac{\partial \mathbf{A}^H(\theta^{RM}, d^{RM})}{\partial d^{RM}}\Big]\mathbf{X} \tag{19}$$

$$\frac{\partial \mathbf{\Pi}}{\partial r^{RM}} = \mathbf{H^{BR}\Omega}\Big[\frac{\partial \mathbf{A}(\phi^{RM}, r^{RM})}{\partial r^{RM}}\rho^{RM} + \mathbf{A}(\phi^{RM}, r^{RM})\frac{\partial \rho^{RM}}{\partial r^{RM}}\Big]\mathbf{A}^H(\theta^{RM}, d^{RM})\mathbf{X} \tag{20}$$

$$\frac{\partial \mathbf{\Pi}}{\partial \phi^{RM}} = \mathbf{H^{BR}\Omega}\frac{\partial \mathbf{A}(\phi^{RM}, r^{RM})}{\partial \phi^{RM}}\rho^{RM}\mathbf{A}^H(\theta^{RM}, d^{RM})\mathbf{X} \tag{21}$$

$$\frac{\partial \mathbf{\Pi}}{\partial \theta^{RM}} = \mathbf{H^{BR}\Omega A}(\phi^{RM}, \hat{r}^{RM})\rho^{RM}\frac{\partial \mathbf{A}^H(\theta^{RM}, d^{RM})}{\partial \theta^{RM}}\mathbf{X} \tag{22}$$

Since all the derivatives are over $\mathbf{A}(\alpha^{RM}, s^{RM})$ and ρ^{RM}, we can write compactly the derivatives over each component as

$$\frac{\partial a_{b,l}(\alpha_l, s_l)}{\partial \alpha} = j\Big[-\frac{2\pi b\delta}{\lambda}\cos(\alpha_l) - \frac{b^2\pi\delta^2}{\lambda s_l}\sin(2\alpha_l)\Big]a_{b,l}(\alpha_l, s_l) \tag{23}$$

$$\frac{\partial a_{bl}(\alpha_l, s_l)}{\partial s} = -j\frac{\pi b^2\delta^2\cos^2(\alpha_l)}{\lambda s_l}a_{b,l}(\alpha_l, s_l) \tag{24}$$

$$\frac{\partial \rho(s_l, d_l)}{\partial s_l} = -\frac{\mu c^{\mu/2}}{2^{\mu+1}\pi^{\mu/2}f^{\mu/2}(s_l + d_l)^{\frac{\mu+2}{2}}}F \tag{25}$$

To transform $\mathbf{J}_\eta$ into $\mathbf{J}_\xi$, we compute the Jacobian matrix $\mathbf{T}$, where $[\mathbf{T}]_{i,j} = \frac{\partial \boldsymbol{\eta}_i}{\partial \boldsymbol{\xi}_j}$.

Using the transformation provided by this Jacobian matrix, we can finally obtain the FIM for the $\boldsymbol{\xi}$ vector as

$$\mathbf{J}_\xi = \mathbf{T}\mathbf{J}_\eta\mathbf{T}^\top \tag{26}$$

where we notice the dependence with the RIS phases through matrix $\mathbf{\Omega}$. This enables the formulation of an optimization problem to obtain the optimal phases by minimizing the trace of the inverse of the FIM for the UE position

$$\hat{\mathbf{\Omega}} = \arg\min_{\Omega}\ \text{tr}(\mathbf{J}_\xi^{-1}) \tag{27}$$

C. Iterative estimation

The UE position estimation involves an iterative process outlined in the algorithm below. Initially, random phases are considered, and through the application of the OMP algorithm, we systematically calculate the geometric parameters. Subsequently, the optimized phases of $\mathbf{\Omega}$ are determined based on the chosen phase optimization method (either *Max. SNR phases method* or *Min. CRLB phases method*). Following this, with the updated RIS matrix, all parameters are recomputed, and the entire process is repeated until convergence.

Algorithm 1 LOCALIZATION ALGORITHM

Require: $\mathbf{H}, \mathbf{X}$, and maximum algorithm iterations K
1: Draw random phases $\mathbf{\Omega}$.
2: **for** $i = 1 : K$ **do**
3: Obtain $\mathbf{V}$ using Equation 7 and compute $\mathbf{V}^H$
4: Build $\mathbf{S}_2$ using the required angles
5: Recover $\mathbf{C}_2$ using OMP and obtain $\hat{\theta}^{RM}$
6: Get $\hat{\phi}^{RM}$ using ($\theta_1^{RM} = \pi + \phi_1^{RM}$)
7: Build the measurement matrix from Equation 11 using the estimated angle
8: Recover $\mathbf{C}_4$ using OMP and get $\hat{d}^{RM}$
9: Compute $\mathbf{\Omega}$ according to Equation 27.
10: **end for**
11: Obtain UE position using Equation 16.

IV. Results

This section provides an analysis on the accuracy of the UE position estimation, focusing on its convergence throughout iterations and, its relation with the transmission SNR and the number of RIS elements (N^R).

Specifically, we will distinguish three cases based on the RIS phases optimization method used: non-optimized (random) phases (*Random phases*), optimized phases maximizing the SNR (*Max. SNR phases method*), and optimized phases minimizing the CRLB (*Min. CRLB phases method*). The fixed parameters are: $x^B = [0, 0]$, $x^R = [5, 5]$, $x^M = [10, 0.5]$, $N^B = 51$, $N^M = 21$, $f_c = 28$ GHz, $\mu = 3$ and $M^0 = 64$. In addition, to obtain the transmitted SNR, thermal noise is considered ($\sigma^2 = B_t K T_k$, with $B_t = 10$ MHz, K being the Boltzmann constant and $T_k = 290$ K).

A. Iterative process (RMSE and SNR)

This subsection describes the empirical behaviour of the RMSE and SNR throughout iterations, for each of the aforementioned methods[3].

On the one hand, Figure 2 depicts a comparative analysis on the evolution of the RMSE given a fixed number of RIS elements ($N^R = 40$). As expected, the use of non-optimized phases results in a high positioning error (on the order of almost 5 meters), coupled with a non-convergent behavior. In contrast, phases optimized maximizing the SNR

[3]Notice that *Random Phases* method employs randomly-generated phases, independently at each iteration.

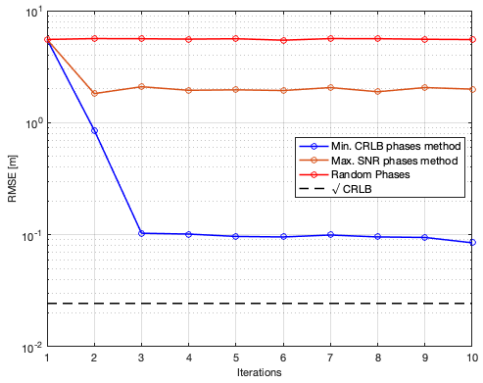

Fig. 2: Evolution of the RMSE throughout iterations (with $N^R = 40$ and SNR $= 20$dB) for the three methods.

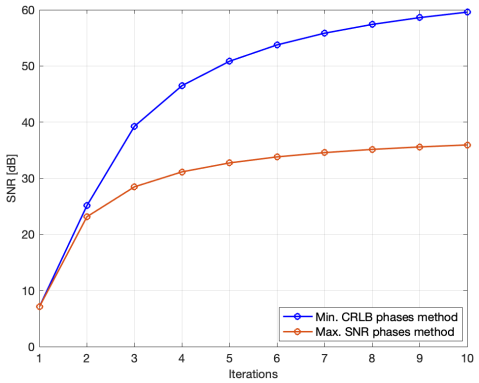

Fig. 3: Evolution of the SNR throughout iterations (with $N^R = 40$ and SNR $= 20$dB) for the three methods.

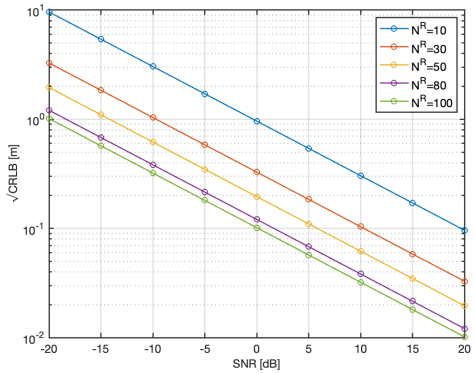

Fig. 4: CRLB as a function of the SNR for different N^R values.) for the three methods.

show higher convergence, achieving in this case an error magnitude of 2 meters approximately. However, the proposed optimization method (*Min. CRLB phases method*) has shown a clear efficacy improvement, with a rapid convergence as well and a substantially higher positioning accuracy comparable to the theoretical CRLB.

On the other hand, given this same scenario, Figure 3 explores the behaviour of the SNR. As the number of iterations increases, there is a corresponding rise in SNR for both methods as expected. Nonetheless, the received SNR achieved by the proposed method exhibits a faster increase, reaching higher values in comparison to the *Max. SNR phases method*.

B. Impact of the RIS number of elements

Theoretically, an increase on the number of reflecting elements in the RIS contributes to enhancing the resolution and, consequently, the positioning accuracy. Figure 4 illustrates how increasing the number of RIS elements results in a lower theoretical CRLB, throughout different SNR values.

This relation between RIS elements and RMSE can be empirically validated, for both iterative methods, as shown in Figure 5. However, this behaviour persists only until $N^R = 40$, beyond which the RMSE stabilizes [4].

Notice that the CRLB is inversely proportional to the number of RIS elements. Hence, this observation implies that the RMSE deviates further from the theoretical bound as N^R increases.

Moreover, Figure 5 leads to a further result. In comparison to *Max. SNR phases method*, obtaining RIS phases through the proposed method is particularly more efficient when the number of RIS elements is increased, showing a significantly lower RMSE value. However, the difference stabilizes after the aforementioned $N^R = 40$.

C. Impact of the SNR

Examining now the relation between the SNR and the CRLB, Figure 4 justifies a theoretical relationship of inverse proportionality between the CRLB and the SNR, holding consistently across different dimensions of the RIS.

In Figure 6, the influence of SNR on RMSE is presented for the two distinct methods. Notably, employing the proposed method yields a substantial reduction in RMSE as SNR increases, converging towards the theoretical bound. In contrast, utilizing the methodology introduced in [15], results in a difference of one order of magnitude between RMSE and the CRLB even for high SNR.

V. Conclusion

In this work, we have developed a RIS phase optimization method based on the minimization of the Cramér-Rao Lower Bound, for 5G systems in a near-field scenario.

The proposed method has shown an improvement with respect to our baseline (i.e. phase optimization through SNR maximization), in terms of positioning accuracy. This outperformance has proven to be robust to the variation of some key system parameters (RIS size N^R and transmission SNR). In addition, we have achieved positioning accuracy values comparable to the theoretical CRLB.

[4]This effect could be attributed to the specific resolution parameters that have been applied to the OMP recovery method.

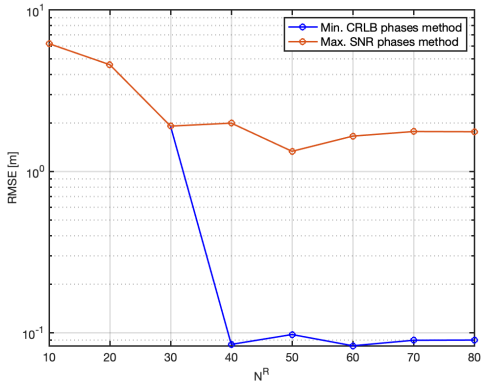

Fig. 5: RMSE as a function of the RIS size for the two studied methods with SNR $= 20$.

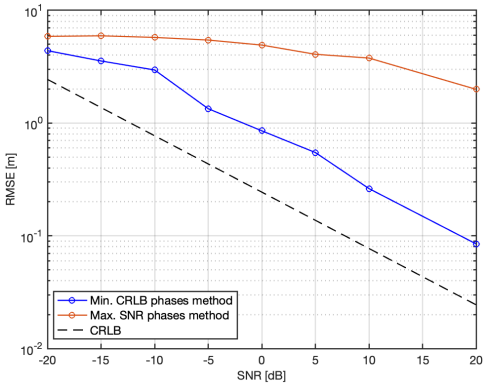

Fig. 6: RMSE as a function of the SNR for $N^R = 40$

These results definitely have room for improvement, specially in terms of computational cost. Hence, further methods could be explored to speed up the minimization process.

VI. Acknowledgement

The UPC authors are within the Signal Processing and Communications Group at UPC recognized as a consolidated research group by the Generalitat de Catalunya through 2021 SGR 01033. This publication is part of the project ROUTE56 with grant PID2019-104945GB-I00 funded by MCIN/AEI/ 10.13039/501100011033 and the project 6-SENSES with grant PID2022-138648OB-I00 funded by MCIN/AEI/ 10.13039/501100011033 and by ERDF A way of making Europe. This work has been partially supported by the National Science Foundation under Awards ECCS-1845833 and CCF-2326559.

References

[1] Davide Dardari, Pau Closas, and Petar M Djurić. Indoor tracking: Theory, methods, and technologies. *IEEE Transactions on Vehicular Technology*, 64(4):1263–1278, 2015.

[2] Xilong Pei, Haifan Yin, Li Tan, Lin Cao, Zhanpeng Li, Kai Wang, Kun Zhang, and Emil Björnson. Ris-aided wireless communications: Prototyping, adaptive beamforming, and indoor/outdoor field trials. *IEEE Transactions on Communications*, 69(12):8627–8640, 2021.

[3] Ali Yassin, Youssef Nasser, Mariette Awad, Ahmed Al-Dubai, Ran Liu, Chau Yuen, Ronald Raulefs, and Elias Aboutanios. Recent advances in indoor localization: A survey on theoretical approaches and applications. *IEEE Communications Surveys Tutorials*, 19(2):1327–1346, 2017.

[4] Haobo Zhang, Hongliang Zhang, Boya Di, Kaigui Bian, Zhu Han, and Lingyang Song. Metalocalization: Reconfigurable intelligent surface aided multi-user wireless indoor localization, 2023.

[5] Marco Di Renzo, Alessio Zappone, Merouane Debbah, Mohamed-Slim Alouini, Chau Yuen, Julien de Rosny, and Sergei Tretyakov. Smart radio environments empowered by reconfigurable intelligent surfaces: How it works, state of research, and road ahead, 2020.

[6] Cunhua Pan, Gui Zhou, Kangda Zhi, Sheng Hong, Tuo Wu, Yijin Pan, Hong Ren, Marco Di Renzo, A. Lee Swindlehurst, Rui Zhang, and Angela Yingjun Zhang. An overview of signal processing techniques for ris/irs-aided wireless systems. *IEEE Journal of Selected Topics in Signal Processing*, 16(5):883–917, 2022.

[7] Miguel Dajer, Zhengxiang Ma, Leonard Piazzi, Narayan Prasad, Xiao-Feng Qi, Baoling Sheen, Jin Yang, and Guosen Yue. Reconfigurable intelligent surface: Design the channel – a new opportunity for future wireless networks, 2020.

[8] Yuhua Jiang, Feifei Gao, Mengnan Jian, Shun Zhang, and Wei Zhang. Reconfigurable intelligent surface for near field communications: Beamforming and sensing. 2022.

[9] Jiguang He, Henk Wymeersch, Tachporn Sanguanpuak, Olli Silvén, and Markku Juntti. Adaptive beamforming design for mmwave ris-aided joint localization and communication, 2019.

[10] Ahmed Elzanaty, Anna Guerra, Francesco Guidi, and Mohamed-Slim Alouini. Reconfigurable intelligent surfaces for localization: Position and orientation error bounds. *IEEE Transactions on Signal Processing*, 69:5386–5402, 2021.

[11] Zohair Abu Shaban, Kamran Keykhosravi, Musa Furkan Keskin, George Alexandropoulos, Gonzalo Seco-Granados, and Henk Wymeersch. Near-field localization with a reconfigurable intelligent surface acting as lens. 10 2020.

[12] Jiguang He, Henk Wymeersch, Long Kong, Olli Silvén, and Markku Juntti. Large intelligent surface for positioning in millimeter wave mimo systems, 2019.

[13] Yiming Liu, Erwu Liu, Rui Wang, and Yuanzhe Geng. Reconfigurable intelligent surface aided wireless localization. pages 1–6, 06 2021.

[14] Mingan Luan, Bo Wang, Yanping Zhao, Zhiyuan Feng, and Fengye Hu. Phase design and near-field target localization for ris-assisted regional localization system. *IEEE Transactions on Vehicular Technology*, 71(2):1766–1777, 2022.

[15] Omar Rinchi, Ahmed Elzanaty, and Mohamed-Slim Alouini. Compressive near-field localization for multipath ris-aided environments. *IEEE Communications Letters*, 26(6):1268–1272, 2022.

[16] Jiguang He, Henk Wymeersch, and Markku Juntti. Channel estimation for ris-aided mmwave mimo systems via atomic norm minimization. *IEEE Transactions on Wireless Communications*, 20(9):5786–5797, 2021.

[17] Sen Li, Bing Li, Bin Lin, Xiaofang Tang, and Rongxi He. Sparse reconstruction based robust near-field source localization algorithm. *Sensors*, 18(4), 2018.

[18] Dror Baron, Michael Wakin, Marco Duarte, Shriram Sarvotham, and Richard Baraniuk. Distributed compressed sensing. 05 2012.

[19] Zhilin Zhang and Bhaskar Rao. Sparse signal recovery with temporally correlated source vectors using sparse bayesian learning. *IEEE Journal of Selected Topics in Signal Processing*, 5:912 – 926, 09 2011.

[20] Jean-François Determe, Jérôme Louveaux, Laurent Jacques, and François Horlin. On the exact recovery condition of simultaneous orthogonal matching pursuit. *IEEE Signal Processing Letters*, 23:164–168, 2015.

[21] Lu Si, Weizhang Xu, Xinle Yu, and Hang Yin. An improved orthogonal matching pursuit algorithm for cs-based channel estimation. *Sensors*, 23(23), 2023.

[22] Teng Ma, Xia Lei, Lechen Zhang, Yun Niu, and George Karagiannidis. Reconfigurable intelligent surface assisted localization: Technologies, challenges, and the road ahead. *IEEE Open Journal of the Communications Society*, PP:1–1, 01 2023.